Available online at www.sciencedirect.com
ScienceDirect
Journal of Power Sources 166 (2007) 68–73
JOURNAL OF POWER SOURCES
www.elsevier.com/locate/jpowsour

Short communication

# Effect of an oxygen plasma treatment on the specific surface of platinum electrodeposits for fuel cells

Nicolas Massoni [a,b,*], Audrey Beaumont-Martinent [b], Jean-Yves Laurent [b]

[a] *Commissariat à l'Energie Atomique (CEA), LETI-DOPT, 17 av. des martyrs, 38054 Grenoble Cedex 9, France*
[b] *Commissariat à l'Energie Atomique (CEA), LITEN-DTNM, 17 av. des martyrs, 38054 Grenoble Cedex 9, France*

Received 28 September 2006; received in revised form 20 December 2006; accepted 28 December 2006
Available online 18 January 2007

**Abstract**

Fuel cells involve electrochemical reactions often catalysed by platinum whose surface has to be maximized. In this paper, platinum nano-particles are deposited onto graphite by a potentiostatic reduction of a dilute 1.0 mM solution of hexachloroplatinate acid. Some samples are pre-treated by highly dissociated oxygen plasma and exhibit an increase of their specific surface compared to the untreated ones. The gain factor on specific surface reaches 3.6 and even 4.4 when the plasma treatment is coupled with the impregnation technique. Surface functionalization made by the plasma treatment lead to denser deposits thanks to an organized nucleation and growth of platinum nuclei. XPS analyses suggest the existence of C–O bonds in the platinum clusters. Although the testing conditions were not optimized, we have measured the performances of a microfuel cell made with the optimized catalyst. The Scharifker and Hills electrocrystallisation model was used to fit the current transients. Untreated samples transients were correctly fitted by the model whereas plasma treated samples transients did not have the requested shape for this model. Hence, nucleation mechanism was determined and confirmed by observation on untreated samples only. The calculated value of the diffusion coefficient of the Pt(IV) anion $PtCl_6^{2-}$ determined by the Cottrell theory was close to the literature, i.e. $2.6 \pm 0.6 \times 10^{-6}$ cm$^2$ s$^{-1}$.


*Keywords:* Platinum electrodeposition; Graphite functionalization; Fuel cells; Scharifker and Hills electrocrystallisation model

## 1. Introduction

Fuel cells (FC) involve oxidation and reduction reactions respectively at the anode and cathode who are generally catalysed by platinum. In order to maximize theses reactions, the surface of the electrodes must be as developed as possible. That is why electrodeposition of platinum nano-particles on conventional electrodes of graphite has been widely studied [1–4]. Hexachloroplatinic acid $H_2Pt(Cl)_6$ [5–7] and pulsed potentiostatic procedure were carried out to realize nano-particles on graphite. As a nucleation layer for an electrodeposition process, graphite exhibits microstructural defects such as step edges. Although they act as nucleation sites [1] and ease a dense nucleation, it has been shown that the induced roughness worsens his natural hydrophobic character [8]. Thus, nucleation and growth mechanisms that rule Pt deposition may be seriously hindered and the process becomes not reliable and reproducible. Some techniques have been reported to tackle this problem: impregnation of the substrate in hexachloroplatinic acid [1,11], thermal oxidation [2] and abrasion [9] of the substrate to produce more nucleation sites. It has been recently pointed out that oxygen plasma treatment of graphite leads to the functionalization of the surface thanks to low energy and high density oxygen radicals [10]: XPS analyses show C–O groups formation and a substantial surface oxidation which both highly improve the wettability of graphite. In this paper we report on a method of electrodeposition based on graphite functionalization by oxygen plasma treatment followed by hexachloroplatinic acid impregnation. Thus, after a several pulsed electrochemical reduction, we obtain platinum nano-particles. Developed surface of the deposit is measured by cyclic voltametry, i.e. by hydrogen adsorption/desorption coulometry. Direct observation of the platinum clusters has been achieved by field effect gun scanning electron microscopy (FEG-SEM) from LEO Company.

* Corresponding author at: Commissariat à l'Energie Atomique (CEA), LETI-DOPT-STM, 17av. des martyrs, 38054 Grenoble Cedex 9, France.
Tel.: +33 438 789 190; fax: +33 438 785 117.
*E-mail address:* nicolas.massoni@cea.fr (N. Massoni).

0378-7753/$ – see front matter © 2007 Elsevier B.V. All rights reserved.
doi:10.1016/j.jpowsour.2006.12.101

## 2. Experimental part

### 2.1. Platinum deposition

Aqueous hexachloroplatinic acid solution at 8 wt.% was purchased from Aldrich and diluted to obtain a 0.001 mol $L^{-1}$ chemical solution. The deposits experiments are carried out in a standard electrochemical three electrodes cell. The working electrode (WE) is a 4 in. silicon wafer oriented ⟨1 0 0⟩ covered with gold and graphite and the counter electrode (CE) is a 4 in. diameter disk of graphite. A 500 nm-thick gold layer is sputtered by PVD onto the wafer with a power source of 50 W. The working electrode typical geometrical surface is 20 $cm^2$ and is partially covered with synthetic graphic plates KS4 from Timcal. All potentials are quoted to the SCE scale. Electrodes are controlled by a Voltalab PST 050 module, interfaced with a computer equipped with the software VoltaMaster 4. Experiments were conducted at room temperature. During deposition oxygen removing by argon bubbling and regular stirring is applied. Measured open circuit potentials (OCP) are from 650 to 800 mV depending whether plasma treatment has been done or not. Desired platinum loadings of 0.1 mg $cm^{-2}$ are achieved using a pulsed potentiostatic method with a large overpotential from 700 to 900 mV. Hydrogen evolution zone is located 100 mV below the deposit potential. At the end of the deposit, samples are removed from the cell, rinsed thoroughly with ultra pure water and transferred to a similar cell with 0.5 M sulphuric acid. Then, cyclic voltametry is undertaken at 10 and 100 mV $s^{-1}$ in the potential range of [−200; 1200] mV to follow hydrogen adsorption and desorption on platinum. Assuming a theoretical adsorption charge of 210 μC $cm^{-2}$, the real surface of the deposit can be deducted. The specific surface $S$ is obtained by dividing the real surface of the deposit by the mass of platinum calculated from the total charge of the deposit using the Faraday electrochemical law. The average particle diameter $d$ in nm is calculated from the specific area $S$ in $m^2\ g^{-1}$ assuming a spherical shape of the particles by the equation $d = 6000/\rho S$ where $\rho$ is the density of platinum 21.4 g $cm^{-3}$ [2].

### 2.2. Plasma device and impregnation

Two process modifications were successively introduced in the standard process (sample #1) to see their impact on specific surface. The first modification is an oxygen plasma treatment before each deposit experiment (sample #2). It has been realized in a microwave discharge device V15-G from Plasma finish GmbH Company. The plasma vessel was an aluminium cubic shaped chamber with an approximate volume of 15 L pumped by a multi stages dry pump from Alcatel with a pumping speed of 7.5 L $s^{-1}$. Samples were laid out on an insulated plate. Typical oxygen flows of 15 sccm were introduced in the chamber and ionized by a microwave radiation at the frequency of 2.45 GHz. Typical applied power and run-time were respectively 350 W and 60 s. The advantage of this electrodeless discharge is that radical density is independent from the ionized species energy. Great densities of highly reactive oxygen dissociated can diffuse onto the substrate providing a chemical treatment without any risk of ion etching. Typical density of oxygen dissociated was about $10^{16}\ m^{-3}$ and the electron temperature about 5.5 eV [10]. The second modification consists in the previously detailed plasma treatment associated to the so called impregnation process where sample is simply immersed in the chemical deposit solution during around one night with OCP monitoring (sample #3). According to the literature [1,11], a chemisorption of platinum should occur leading to a small charge of platinum weak bonded with the substrate of graphite. We observed a linear increasing of the OCP during the impregnation. The final value of the OCP is the same value that we could measure for a platinum surface immersed in the chemical deposit solution. It strongly suggests that platinum covers the graphite after the impregnation. The same electroreduction steps are applied to the substrate for the three samples.

### 2.3. XPS measurements

XPS analyses were made several days after the deposition of the platinum. The device used was an S-Probe model from Surface Science Instrument. The samples were excited by a monochromatic Al Kα at 1486.6 eV with a spot size of 250 μm × 1000 μm for the general analyses. A smaller spot size of about 150 μm × 800 μm is preferred for detailed analyses. The base pressure in the analysis chamber was about $10^{-9}$ mbar. Photoelectrons were collected with a standard hemispherical electrostatic analyzer. An energy resolution of 0.85 eV was measured on a gold reference sample. Hence, binding energies until 1000 eV were detected.

## 3. Results and discussions

### 3.1. Effect of the plasma treatment on the specific platinum surface

The results are summarized in Table 1. As a basis, standard process exhibits a low specific surface (sample #1). It is increased by a factor 3.6 thanks to plasma treatment (sample #2). This point could be explained by a more favourable nucleation. Fig. 1 compares nucleation of platinum onto surfaces which were treated (Fig. 1A) and untreated by plasma (Fig. 1B). Fig. 2 represents hydrogen adsorption coulometry curves carried out in the $H_2SO_4$ solution to determine their specific surfaces reported in Table 1. The deposits show a granular morphology. It shows a more homogeneous nucleation for plasma treated samples than the untreated ones for a same loading of platinum of 100 μg $cm^{-2}$. Platinum nano-particles of the untreated sample (#1) have different sizes from 10 to 50 nm while the treated samples (#2 and #3) exhibit smaller and similar-sized nano-particles of an average diameter of 6 nm. Nuclei agglomeration seems to be less present as well; it might be due to the better dispersion obtained during the first stage of the deposit. In the same way, surface modification was revealed by different electrodeposition curves for samples #1 and #3 (Section 3.3, Fig. 5). Kinetic deposit was also accelerated thanks to a doubled current density. The functionalization made by oxygen neutral atoms during plasma treatment has probably modified the sur-

Table 1
Specific surfaces of the various samples for a constant platinum loading of 100 μg cm$^{-2}$

| Sample | Oxygen plasma | Impregnation | Specific surface $S$ (m$^2$ g$^{-1}$) | Measured particle diameter $d$[a] (nm) |
|---|---|---|---|---|
| #1 | | | 11 ± 3 | 10–50 [25] |
| #2 | X | | 40 ± 4 | <10 [6.6] |
| #3 | X | X | 48 ± 5 | 6 [5.8] |

[a] Expected diameters in brackets are calculated from the specific surface. Bad imaging conditions seldom allow us precise measures.

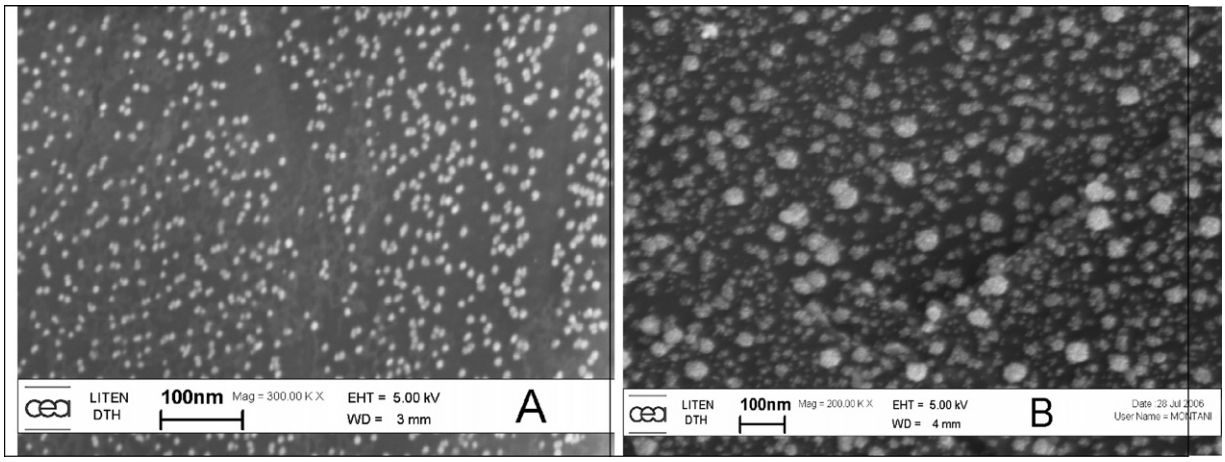


Fig. 1. Different densities of nucleation of platinum on graphite with the same loading of platinum of 100 μg cm$^{-2}$ for A, plasma treated sample #3 and B, plasma untreated sample #1. On picture A, the average diameter measured is 6 nm, close to the theoretical value of 5.8 nm calculated from the specific area as listed in Table1. On picture B, the calculated diameter of 25 nm seems to be the mean diameter of the clusters.

face deposit by creation of C–O groups on graphite according to Cvelbar et al. [10]. For these authors, the involved wettability enhancement improved the electrocrystallisation process that occurs onto graphite. The C–O groups may have acted as more favourable nucleation sites allowing a better distribution of platinum clusters. It has lead to an undoubtedly smaller deposit as shown in Fig. 1A. We can see that impregnation improves the specific area by a factor 1.2 for plasma treated samples (Table 1, #2 and #3); that is less important than previously reported by Gloaguen and al. [2], i.e. a factor 2, on untreated samples. The intimate and prolonged contact of the functionalized surface during impregnation has lead to a better chemisorption of platinum. Sample #3, where plasma and impregnation were done, exhibits the highest specific surface of 48 m$^2$ g$^{-1}$. Assuming a spherical shape of the cluster, the theoretical diameter calculated is 5.8 nm; very close to the estimated value of 6 nm in Fig. 1A namely approximately a cluster formed by 180–240 atoms. We are far from the critical cluster size of 30–40 atoms, i.e. a diameter of 1 nm reported by Chen and Kucernak [3].

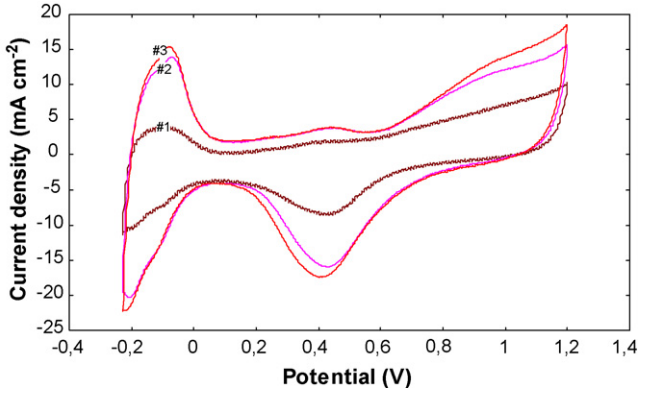


Fig. 2. Voltamperograms recorded in 0.5 M $H_2SO_4$ at 100 mV$^{-1}$ for samples without plasma (#1), with plasma treatment (#2, 3) for a same platinum loading of 0.4C.

### 3.2. Platinum bond with the functionalized surface

The Pt binding spectrum of plasma untreated and treated samples (Fig. 3) did not point out any differences. According to the literature, PtO shifts the Pt peak about 3 eV. Hence, there is no peak which can be assigned to a platinum oxide. However, some authors [20] fix this shift to 1 eV. Following this last rule, there could be a peak assigned to platinum oxide. Nevertheless the absence of a clear Pt–O peak can be due to either the small part

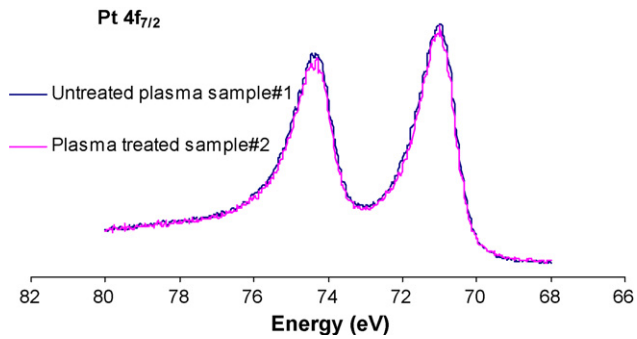


Fig. 3. Platinum XPS spectra for untreated and plasma treated samples.

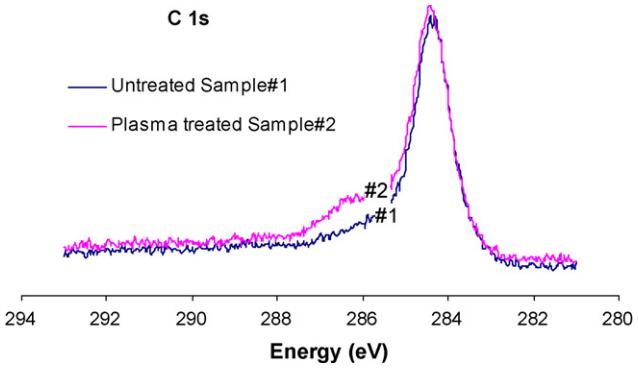


Fig. 4. Oxygen XPS spectra for untreated and plasma treated samples.

Table 2
Proposed equations for current time transients modelling for a 3D nucleation according to the Scharifker and Hills theory

| Nucleation mechanism | Equations | |
|---|---|---|
| Progressive | $I = zFc\left(\frac{D}{\pi t}\right)^{1/2}[1 - \exp(-0.5 \times AN_{\infty}\pi k' Dt^2)]$ | (1) |
| | with $k' = \frac{4}{3}\left(\frac{8\pi cM}{\rho}\right)^{1/2}$ | (2) |
| Instantaneous | $I = zFc\left(\frac{D}{\pi t}\right)^{1/2}[1 - \exp(-N\pi k Dt)]$ | (3) |
| | with $k = \left(\frac{8\pi cM}{\rho}\right)^{1/2}$ | (4) |

of Pt–O bonds that is under the detection limit of the device or there is the size effect of the nano-particles. Indeed the XPS peaks database is built from bulk measurements and significant differences of energy shifts values have been already observed, especially for nano-particles of silicon [19]. Hence, we cannot know how platinum is connected with the surface. The observation of the C 1s spectrum shows a little difference at 286 eV in Fig. 4.

According to the literature, this peak is assigned to C–O bond. We can confirm the work of Cvelbar et al. [10] concerning the creation of C–O bonds thanks to highly dissociated oxygen plasma. The deconvoluated spectra show us that even untreated sample has C–O groups whereas the plasma treated sample has a around twice more C–O groups than the untreated one (Fig. 5). Although Pt–O bonds have not been clearly detected, we strongly suppose the existence of Pt–O–C bonds.

### 3.3. Scharifker and Hills electrocrystallisation model

Scharifker and Hills developed a model for 3D nucleation with diffusion controlled growth under potentiostatic control [12], successfully applied to current time transients to obtain several parameters of the deposit [2,21,22] such as the diffusion coefficient of the specified ion. Based on the overlapping of hemispherical diffusion zones, this model is suitable only for samples where current time transients have the expected shape [12]. The authors considered that the first stage of the nucleation is made with randomly distributed hemispherical nuclei. The diffusion along the surface was not discussed in this model; the nuclei have found their final nucleation site. Then, two mechanisms of nucleation can be taken in account: either the nuclei are created simultaneously, their number remains constant and their growth rate is the same, the nucleation mechanism is known to be instantaneous. It leads to a layer morphology of clusters having the same size. Or the nuclei are constantly being formed and they grow to different sizes and/or at different rates, the nucleation is called progressive and the related expected morphology is clusters having significant different sizes. According to the model, the current transients can be represented by the following equations [22] in Table 2. Where $n$ is the number of electrons, $F$ the Faraday's constant, $D$ the diffusion coefficient, $c$ the bulk concentration of the electroactive ion, $M$ the molecular weight of the metal ion, $\rho$ the metal density, $N$ the number of nuclei and $AN_{\infty}$ is the nucleation rate. A more practical way to distinguish between the two mechanisms is to represent the transients in a non-dimensional plot, $(I/I_{max})^2$ versus $t/t_{max}$, where $I_{max}$ and $t_{max}$ are the coordinates of the current maximum (Table 3), and to compare these with the following theoretical plots [12] resulting from the equations of Table 2. Assuming the following current time transients shapes shown in Fig. 6, we see that only the sample #1 has the expected shape for a 3D nucleation as required by the Scharifker and Hills theory. The non-dimensional plot is

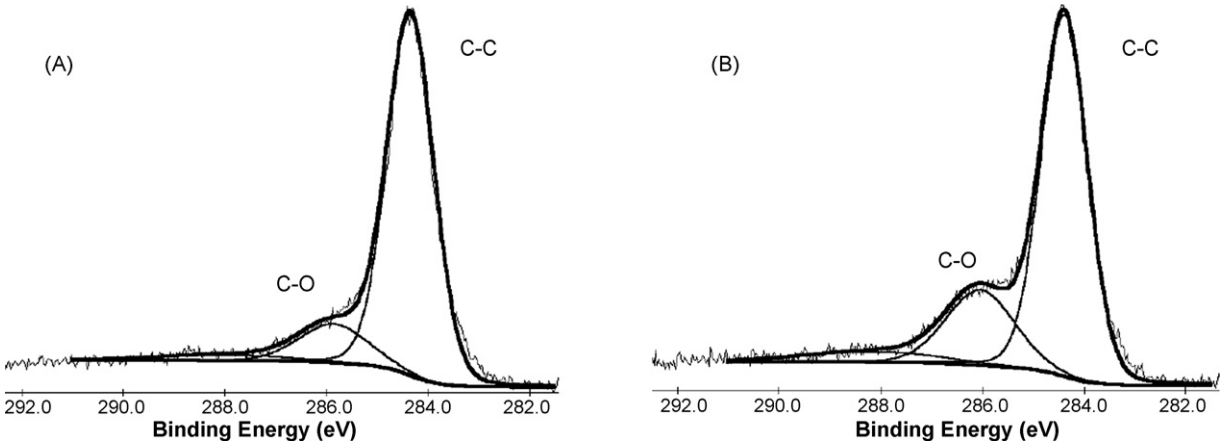


Fig. 5. Spectra of the Fig. 4 after deconvolution for samples after platinum deposition A. untreated and B. plasma treated.

Table 3
Expressions of the equations of the Table 2 in a non-dimensional plot.

| Nucleation mechanism | Equations | |
|---|---|---|
| Progressive | $\left(\frac{I}{I_{max}}\right)^2 = \frac{1.2254}{t/t_{max}}\left\{1-\exp\left(-2.3367\left(\frac{t}{t_{max}}\right)^2\right)\right\}^2$ | (5) |
| Instantaneous | $\left(\frac{I}{I_{max}}\right)^2 = \frac{1.9542}{t/t_{max}}\left\{1-\exp\left(-1.2564\left(\frac{t}{t_{max}}\right)\right)\right\}^2$ | (6) |

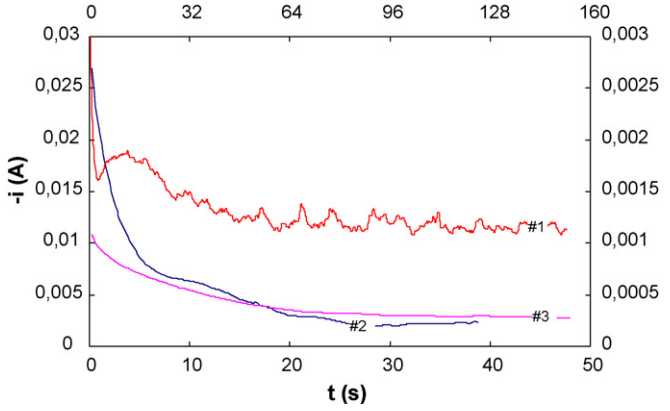


Fig. 6. .Current-time transients of the three samples recorded in 1 mM $H_2PtCl_6$ at -142 mV for a fixed charge of 0.4C. Only the transient of the sample #1 has been represented in non-dimensional plots on Fig. 7. The upper and right scales are for sample #1; the lower and left scales are for samples #2 and #3.

represented in Fig. 7. We tried unsuccessfully to apply the same treatment to the transient of sample #2 because of its shape has a small shoulder around 10 s which can be assigned to a low 3D nucleation effect. The shape of the transient of the sample #3 is typical of a pure planar diffusion control. Thus, nucleation mechanism is not the same for the three samples even if the substrates and experimental conditions were the same. We suggest that plasma treatment and impregnation have lead to a faster nucleation confirmed by the reduction of the deposit time of a factor 4: from 152 s for sample #1 to 48 and 38 s for samples #2 and #3, respectively. Assuming that $t_{max} = 12$ s and $I_{max} = 0.00189$ A for

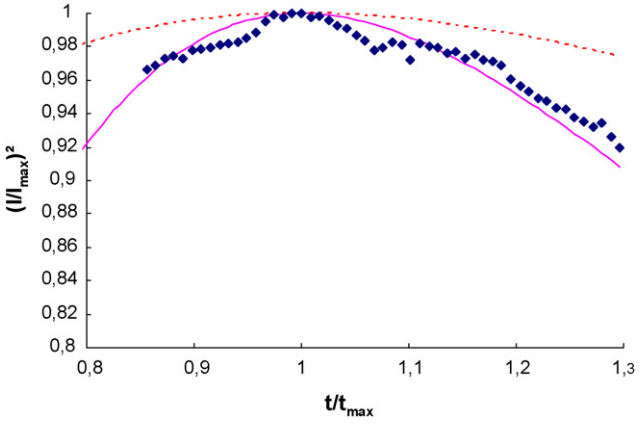


Fig. 7. Non-dimensional plot $(I/I_{max})^2$ vs $t/t_{max}$ of the data of sample #1 of Fig 6. The experimental plot (t) fits the continuous line (-) which corresponds to progressive nucleation whereas the dotted line (- - -) corresponds to the instantaneous nucleation.

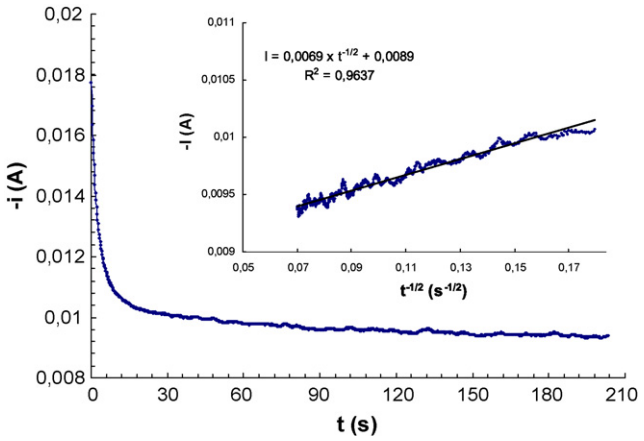


Fig. 8. Typical current-time transient acquired on a surface of 20cm$^2$ of graphite in 1 mM $H_2PtCl_6$. The small capacitive part was removed for the further exploitation. Inset: plot of the current vs time-1/2 according to the Cottrell equation. The diffusion coefficient extracted from this curve gives a value of $2.6 \pm 0.6 \times 10^{-6}$ cm$^2$ s$^{-1}$.

sample #1, Fig. 7 shows the non-dimensional plot of the related transient whose nucleation mechanism is progressive. It is well confirmed by Fig. 1B where observation of nuclei with different diameters has been performed and is generally linked to a progressive nucleation [22].

### 3.4. Cottrell theory

A typical current time transient is shown in Fig. 8. The shape of the curve suggests a planar diffusion control where current evolution is linear with time$^{-1/2}$ (see inset). According to the Cottrell theory, the diffusion coefficient of the Pt(IV) anion $PtCl_6^{2-}$ can be extracted from the slope of the linear plot. This processing yields a diffusion coefficient of $(2.6 \pm 0.6) \times 10^{-6}$ cm$^2$ s$^{-1}$ which is lower but close to the values reported previously, e.g. $4.5 \times 10^{-6}$ cm$^2$ s$^{-1}$ [3,14], $3.4 \times 10^{-6}$ cm$^2$ s$^{-1}$ [2], $5.47 \times 10^{-5}$ cm$^2$ s$^{-1}$ [15], and $5.89 \times 10^{-6}$ cm$^2$ s$^{-1}$ [1]. This may be explained by a kinetic limitation of the $PtCl_6^{2-}$ anion due to the excessive roughness of the graphite or the inhibiting effect of chloride ions released in the course of chloride platinum complexes. After their reduction, six chloride ions are forced off the surface but the $PtCl_6^{2-}$ flow can lead to the incorporation of some of them. Performed EDX spectra reveal indeed the presence of chlorine atoms in the deposit. Although they are known to have a poisonous behavior for platinum catalyst [17,18], the relative small amount of chlorine allows us to conclude that its bad effect is very limited. Another possible limiting factor is the formation of the intermediate complex Pt(II) anion $PtCl_4^{2-}$ as reported by Kravtsov [16]. Because of a controversial and insufficient literature, this eventuality has not been considered.

## 4. Performance of a microfuel cell embedding the optimized catalyst

We have fabricated a microfuel cell with platinum nanoparticles as an anodic catalyst layer with the sample 3. We have

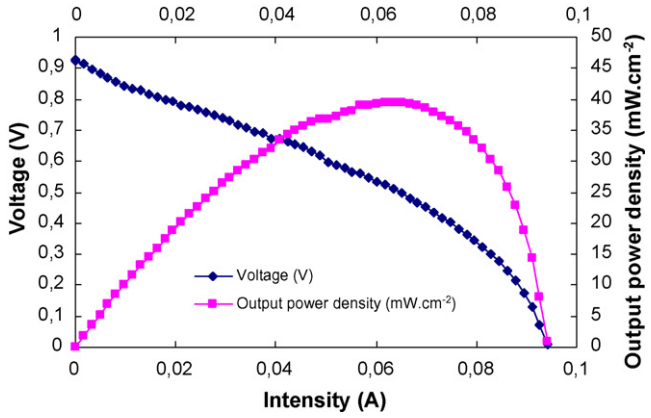


Fig. 9. Performances of the microfuel cell with the nano-particles catalyst. The voltage supplied by the microfuel cell is represented with the diamond-shaped plot (♦) corresponding to the left scale. The output power density is marked with the rectangular plot (■) and is in relation with the right scale.

seen that platinum nano-particles have a larger specific surface which means more available surface for hydrogen reduction. Then, we should observe a gain in the output density power. Fig. 9 shows the voltage supplied by the fuel cell and the output density power respectively as a function of the operating current. These characterizations are undertaken under a hydrogen flow of 10 $cm^3\,min^{-1}$ and the fuel cell is at room temperature. The oxygen source is provided by static and non-humidified ambient air which is not an ideal condition. The measured peak power density is about 40 $mW\,cm^{-2}$ whereas the shunt intensity is approximately 115 $mA\,cm^{-2}$. However, we have experienced many technological problems on the other parts of the microfuel cells which should be the origin of the poor performance. More particularly the need of a better electrolyte membrane has emerged in order to maximize the number of active catalyst points, i.e. where electrolyte, graphite and hydrogen gather. Further experiments are planned to solve these problems and get the expected gain on performance.

## 5. Conclusion

We observed an increase of the specific surface of platinum deposits for samples pre-treated by oxygen plasma. Indeed starting with a process leading to a specific surface of 11 $m^2\,g^{-1}$, we gained a 3.6 factor on the specific surface, i.e. 40 $m^2\,g^{-1}$. By adding the impregnation technique we reached 48 $m^2\,g^{-1}$ confirmed by the direct observation of 6 nm platinum nano-particles. The functionalization of graphite has lead to a better and more organized nucleation and growth of platinum nuclei. XPS analyses suggest that platinum is bonded with the oxygen provided by the plasma treatment. The natural hydrophobic graphite behavior is supposed to be eliminated by the plasma treatment as well and enhances the wettability of the graphite during the deposition. Compared to other treatments such as abrasion, plasma involves neither thermal nor mechanical stress of the substrate with our specified parameters and equipment. Moreover, functionalization can be tuned easily by changing applied power or run-time. It appears that impregnation technique can be coupled with plasma treatment since the combined effect is positive. The performance of a microfuel cell made with the optimized catalyst under non-optimal experimental conditions is about 40 $mW\,cm^{-2}$ which validates the activity of the nano-particles. The findings of this study support Scharifker and Hills electrocrystallisation model, since its boundary conditions are fulfilled. We found that nucleation mechanisms and kinetic were different for the treated and untreated plasma samples.

Functionalization by highly dissociated radical plasma pretreatment is then a promising way to obtain high specific surface deposits. A considerable interest should grow for the coupled technique (plasma plus impregnation) as far as the electrodeposition process may be much more optimized (experiments in progress).

## Acknowledgments

One of the authors (NM) would like to acknowledge the Optronic Department of the CEA for the financial support provided. We also thank Mr. Alexandre Montani for his skills in SEM imagery and Mr. François Pierre for fruitful discussions about XPS.

## References

[1] J.V. Zoval, J. Lee, S. Gorer, R.M. Penner, J. Phys. Chem. B 102 (1998) 1166.
[2] F. Gloaguen, J.-M. Léger, C. Lamy, A. Marmann, R. Vogel, Electrochim. Acta 44 (1999) 1805.
[3] S. Chen, A. Kucernak, J. Phys. Chem. B 107 (2003) 8392.
[4] M.M.E. Duarte, A.S. Pilla, J.M. Sieben, C.E. Mayer, Electrochem. Commun. 8 (2006) 159.
[5] K. Shimazu, K. Uosaki, H. Kita, J. Electroanal. Chem. (1983) 237.
[6] F. Gloaguen, J.-M. Léger, C. Lamy, J. Appl. Electrochem. 208 (1997) 1052.
[7] K.H. Choi, H.S. Kim, T.H. Lee, J. Power Sources 75 (1998) 230.
[8] L. Ostrovskaya, A. Podesta, P. Milani, V. Ralchenko, Europhys. Lett. 63 (3) (2003) 401.
[9] N. Rajalakshmi, H. Ryu, K.S. Dhathathreyan, Chem. Eng. J. 102 (2004) 241.
[10] U. Cvelbar, B. Markoli, I. Poberaj, A. Zalar, S. Spaić, Appl. Surf. Sci. 253 (4) (2006) 1861.
[11] S. Adora, Y. Soldo-Olivier, R. Faure, R. Durand, J. Phys. Chem. B 105 (2001) 10489.
[12] B.R. Scharifker, G. Hills, Electrochem. Acta 28 (1983) 879.
[14] J.L. Zubimendi, L. Vazquez, P. Ocon, J.M. Vara, W.E. Triaca, R.C. Salvarezza, A.J. Arvia, J. Phys. Chem. 97 (19) (1993) 5095.
[15] A. Kelaidopoulou, G. Kokkidinis, J. Electroanal. Chem. 444 (1998) 195.
[16] V.I. Kravtsov, Russian J. Electrochem. 36 (2000) 1209.
[17] T.J. Schmidt, U.A. Paulus, H.A. Gasteiger, R.J. Behm, J. Electroanal. Chem. 508 (2001) 41.
[18] H. Kim, N.X. Subramanian, B.N. Popov, J. Power Sources 138 (2004) 14–24.
[19] O. Renault, R. Marlier, M. Gely, B. De Salvo, Appl. Phys. Lett. 87 (2005) 163119.
[20] Z.R. Yue, et al., Carbon 37 (1999) 1607.
[21] C.S. Barin, A.N. Correia, S.A.S. Machado, L.A. Avaca, J. Braz. Chem. Soc. 11 (2000) 2.
[22] A.N. Correia, S.A.S. Machado, L.A. Avaca, J. Electroan. Chem. 488 (2000) 110.